The 8th European Congress on Computational Methods in Applied Sciences and Engineering
ECCOMAS Congress 2022
5-9 June 2022, Oslo, Norway

VOLUME-OF-FLUID SIMULATION OF THREE-DIMENSIONAL GRAVITATIONAL LIQUID SHEET FLOWS

Alessandro Della Pia[1], Luigi Grande[1], Antonio Colanera[1], Matteo Chiatto[1] and Luigi de Luca[1]

[1] Department of Industrial Engineering, Aerospace Sector,
Università degli Studi di Napoli "Federico II", Naples, 80125, Italy

Key words: interfacial flows, computational fluid dynamics, linear stability analysis.

Abstract. The volume-of-fluid (VOF) method is employed to simulate the dynamics of gravitational liquid sheets (curtains) issuing into an initially quiescent gaseous environment. The flow behaviour is investigated by varying two governing parameters, namely the sheet aspect ratio, $AR = W_i^\star / H_i^\star$, and the Weber number, $We = \rho_l U_i^{\star 2} H_i^\star / (2\sigma)$, where $H_i^\star$ and $W_i^\star$ are the curtain inlet thickness and width, respectively, $U_i^\star$ the inlet mean liquid velocity, ρ_l and σ the liquid density and surface tension coefficient. For a reference Weber number greater than one, three different aspect ratio values are considered, namely $AR = 40$, 25 and 10, and it is found that a varicose mode progressively arises as AR decreases, dramatically affecting the flow at $AR = 10$. The analysis performed by varying We reveals that a stable liquid sheet can be obtained in both supercritical ($We > 1$) and subcritical ($We < 1$) regimes, down to $We = 0.8$, where rupture mechanisms (holes formation and their amplification) start to occur. Linear stability analysis predictions of the sheet oscillation frequency based on a simplified linear low-dimensional model of the flow system are found to be in good agreement with corresponding values arising from the three-dimensional simulations.

1 INTRODUCTION

Gravitational liquid sheets (curtains) interacting with an external gaseous environment are flows of both scientific and industrial interest, due to a wide scenario of applications ranging from paper making (Soderberg and Alfredsson [1]) to coating processes (Weinstein and Ruschack [2]), from space industry (Chubb *et al.* [3]) to waterfall noise reduction (Lodomez *et al.* [4]). Notwithstanding the efforts dedicated by the scientific community to the study of the subject, which are summarized in the literature reviews reported within the historical works by de Luca [5] and Finnicum *et al.* [6], and in the more recent contribution by Torsey *et al.* [7], several issues concerning gravitational liquid curtains dynamics remain open nowadays; one of them consists in the identification of the physical mechanisms leading to the sheet break-up when the inlet volumetric flow rate $Q^\star$ reduces.

As an intermediate step towards a deeper understanding of the physics of curtain rupture, this work presents results of a parametric numerical analysis of the liquid sheet behaviour performed by varying two governing parameters of the flow system, namely the liquid sheet aspect ratio, $AR = W_i^\star / H_i^\star$, and the Weber number $We = \rho_l U_i^{\star 2} H_i^\star / (2\sigma)$, where $H_i^\star$ and $W_i^\star$ are the curtain

inlet thickness and width, respectively, $U_i^\star$ the inlet mean liquid velocity, ρ_l and σ the liquid density and surface tension coefficient. Both the latter dimensionless parameters are related to $Q^\star = U_i^\star W_i^\star H_i^\star$; for a fixed $U_i^\star$, by reducing AR and/or We, the volumetric flowrate also reduces, and the sheet approaches rupture conditions (Brown [8]). The transition of the flow from supercritical ($We > 1$) to subcritical ($We < 1$) conditions is also analyzed by means of linear stability analysis based on a simplified low-dimensional model of the flow, providing comparisons with results arising from the three-dimensional volume-of-fluid (VOF) simulations.

The work is organized as follows: in Section 2, the numerical simulation framework and the flow system details are presented; Section 3 reports and discusses results of the parametric analysis performed by varying AR and We, while conclusions are drawn in Section 4. Further details regarding linear stability analysis calculations are finally provided in Appendix A.

2 VOF SIMULATION OF THREE-DIMENSIONAL LIQUID CURTAINS

2.1 Numerical method

The two-phase flow represented by the liquid curtain interacting with an external gaseous environment is computed within the one-fluid formulation of incompressible Navier-Stokes equations (Scardovelli and Zaleski [9])

$$\frac{\partial u_i^\star}{\partial x_i^\star} = 0, \tag{1}$$

$$\rho\left(\frac{\partial u_i^\star}{\partial t^\star} + u_j^\star \frac{\partial u_i^\star}{\partial x_j^\star}\right) = -\frac{\partial p^\star}{\partial x_i^\star} + \rho g_i + \frac{\partial}{\partial x_j^\star}\left[\mu\left(\frac{\partial u_i^\star}{\partial x_j^\star} + \frac{\partial u_j^\star}{\partial x_i^\star}\right)\right] + \sigma\kappa^\star n_i \delta_S, \tag{2}$$

$$\frac{\partial C}{\partial t^\star} + \frac{\partial C u_i^\star}{\partial x_i^\star} = 0, \tag{3}$$

with $\mathbf{u}^\star = (u^\star, v^\star, w^\star)$ and $\mathbf{g} = (g, 0, 0)$ representing the velocity and gravity acceleration vectors, respectively, $p^\star$ the pressure, σ the surface tension coefficient, $\kappa^\star$ the mean interface curvature, $\mathbf{n} = (n_x, n_y, n_z)$ the outward pointing normal vector and δ_S a Dirac distribution function, equal to 1 at the gas-liquid interface and 0 otherwise. Note that all the dimensional quantities, except gravity acceleration g and fluid material properties (ρ_l, ρ_a, μ_l, μ_a, σ), are denoted with the superscript $\star$. The density ρ and viscosity μ fields are discontinuous across the interface separating the two fluids:

$$\rho = \rho_a + (\rho_l - \rho_a)C, \tag{4}$$

$$\mu = \mu_a + (\mu_l - \mu_a)C, \tag{5}$$

where subscripts l and a refer to liquid and ambient phases, and C is the volume fraction field, equal to 1(0) in the liquid (gaseous) region, respectively. The finite volume method implemented in the open-source code BASILISK (`http://basilisk.fr`) is employed to solve Eqs. (1)-(3). The code implements the volume-of-fluid (VOF) method by Hirt and Nichols [10] to track the interface on an octree structured grid, allowing for adaptive mesh refinement based on a criterion of wavelet-estimated discretization error (van Hooft *et al.* [12]), with no special treatment required in presence of liquid phase break-up. A multigrid solver is employed to satisfy the incompressibility condition, while the calculation of the surface tension term is based

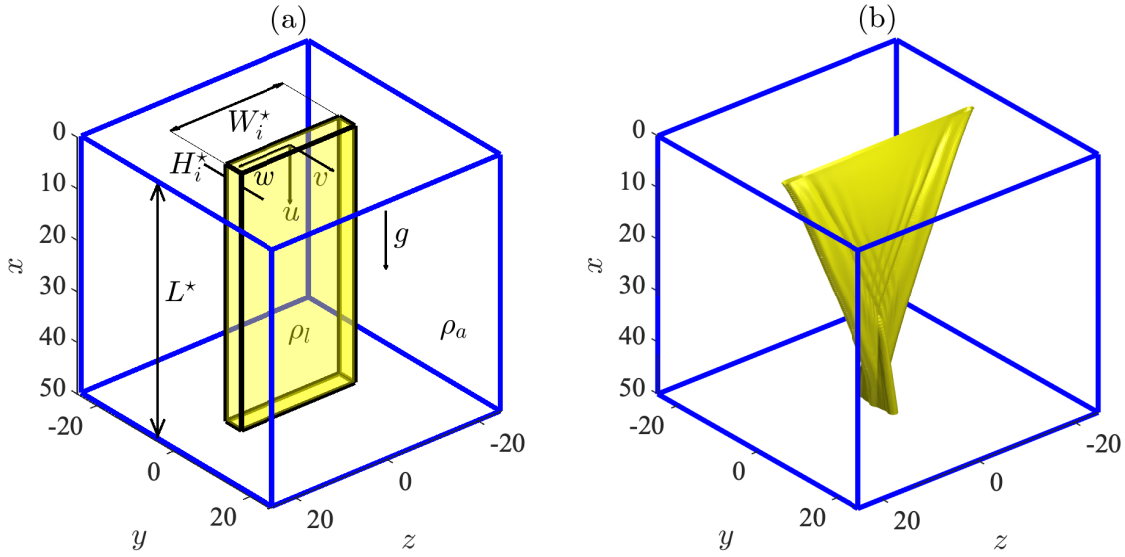

Figure 1: Sketch of computational domain (a) and three-dimensional volume fraction field (b). Note that gravity g is directed along the streamwise x direction, which is represented vertically. $We = 2.5$, $AR = 40$.

on the balanced continuum surface force technique (Francois *et al.* [11]), which is coupled with a height-function curvature estimation to mitigate the generation of spurious currents. For exhaustive details about BASILISK, the reader is referred to Popinet [13, 14].

2.2 Problem formulation

A sketch of the computational domain is reported in Fig. 1(a), where the gravity direction x is represented vertically. It consists in a cubic $[0, L^\star] \times [-L^\star/2, L^\star/2] \times [-L^\star/2, L^\star/2]$ flow region in the x (streamwise), y (transverse) and z (spanwise) directions, where $L^\star = 50H_i^\star$ is also equal to the liquid sheet length. The spatial coordinates x, y and z have been scaled with respect to the initial sheet thickness $H_i^\star$ (for example, $x = x^\star/H_i^\star$), while the corresponding streamwise u, transverse v and spanwise w velocity components have been made dimensionless with respect to the inlet (i.e., at the streamwise station $x = 0$) mean liquid velocity $U_i^\star$ (e.g. $u = u^\star/U_i^\star$).

The curtain issues into an initially quiescent gaseous environment from a rectangular slot of dimensions $W_i^\star \times H_i^\star$, representing the initial width (i.e., extension along the spanwise z direction) and thickness (transverse y dimension) of the sheet, respectively. The mean point of the slot also coincides with the origin of the reference frame, and the curtain shape is initialized as a $L^\star \times H_i^\star \times W_i^\star$ parallelepiped (yellow region in Fig. 1(a), where $C(x, y, z, 0) = 1$), which is employed to start the computation. Following Kacem [15], Dirichlet boundary conditions are enforced at the inlet: in the liquid region (i.e., for $-1/2 < y < 1/2$ and $-AR/2 < z < AR/2$, being $AR = W_i^\star/H_i^\star$ the sheet aspect ratio) a fully developed parabolic velocity profile with an error function modification at the slot boundaries (i.e., at $y = \pm 1/2, z = \pm AR/2$) is imposed,

and the conditions read

$$u = \frac{3}{2}\left(1-4y^2\right)\operatorname{erf}\left(\frac{AR}{2}-z\right)\operatorname{erf}\left(\frac{AR}{2}+z\right), \tag{6}$$

$$v = w = 0, \tag{7}$$

$$C = 1, \tag{8}$$

while a no-slip condition is imposed on the remaining part of the inlet plane (i.e., within the gaseous phase). The four lateral boundary planes ($y = \pm 25, z = \pm 25$) are equipped with homogeneous Neumann boundary conditions for all variables, and on the outlet plane ($x = 50$) a standard outflow condition

$$\frac{\partial u}{\partial x} = \frac{\partial v}{\partial x} = \frac{\partial w}{\partial x} = \frac{\partial C}{\partial x} = 0, \tag{9}$$

$$p = 0, \tag{10}$$

is considered. The same $u(y, z)$ profile adopted as inlet boundary condition (Eq. (6)) is used as initial velocity distribution throughout the entire sheet length, and we explicitly note that Eq. (10) for the differential pressure reproduces the far downstream condition, meaning that the atmospheric pressure is recovered at relatively large downstream stations. The computational domain is discretized with an adaptive mesh up to a maximum number of 2^9 grid points along each spatial dimension, corresponding to a minimum mesh size $\Delta^\star \approx H_i^\star/11$, and approximately 134 million cells if an uniform grid was used. Note that a lower (dimensionless) resolution, corresponding to $\Delta^\star/H_i^\star \approx 6$, has been recently used and shown to be valuable in capturing holes expansion and collision in a thin ($H_i^\star = 25 \cdot 10^{-6}$ m) liquid sheet (Agbaglah [17]). For exhaustive details about the adaptive grid refinement strategy the reader is referred to van Hooft *et al.* [12].

This section is concluded with a brief description of the typical shape adopted by the falling liquid curtain in stable supercritical conditions ($We = 2.5$), once a steady regime is achieved after computations start from the parallelepiped initial condition previously described. The three-dimensional volume fraction field $C(x, y, z)$ obtained for $AR = 40$ (the liquid issues from a slot located at $-20 < z < 20$) is shown in Fig. 1(b), and reveals the characteristic triangular sheet shape outlined by previous theoretical analyses and experimental investigations (among others, Chubb *et al.* [3] and Kacem *et al.* [16]), which is a consequence of the curtain rims retraction and convergence towards the central axis ($x = 0$) due to the effect of surface tension.

3 RESULTS

The aim of this section is to examine the effect of the governing parameters AR and We on the liquid curtain shape and dynamics, providing physical insights into steady and unsteady flow features. Both parameters are related to the volumetric flow rate $Q^\star = U_i^\star H_i^\star W_i^\star$, which decreases both with AR (i.e., by reducing $W_i^\star$) and We (by decreasing $U_i^\star$). For relevant conditions, the three-dimensional VOF results are also compared with predictions from linear stability analysis based on a simplified one-dimensional model of the flow system, to highlight analogies with recent low-order analyses of the curtain dynamics (Della Pia *et al.* [18, 19]).

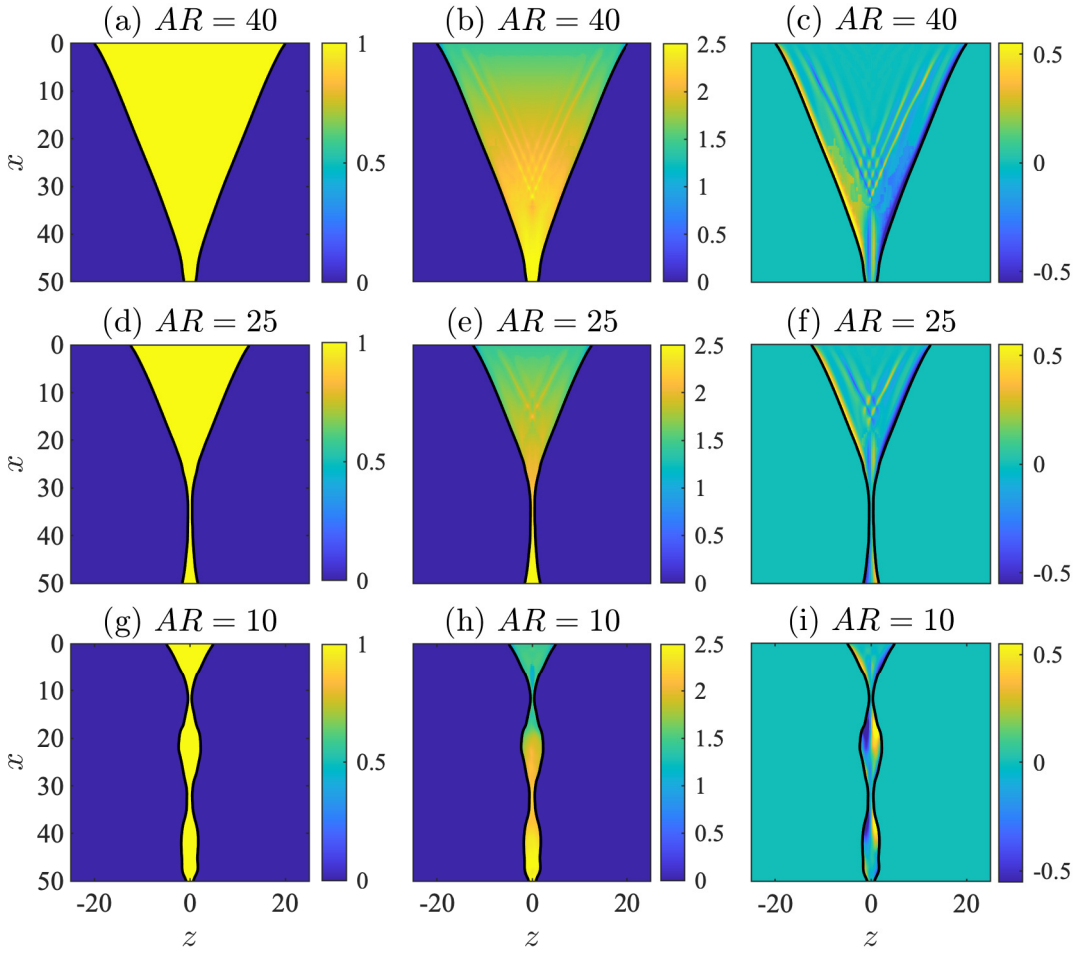

Figure 2: Volume fraction C (first column), streamwise u (second column) and spanwise w (third column) liquid velocity components at different values of the aspect ratio AR in xz plane: $AR = 40$ (panels (a)-(c)), 25 (panels (d)-(f)) and 10 (panels (g)-(i)). $We = 2.5$.

3.1 Effect of the curtain aspect ratio

The effect of aspect ratio variation on the liquid curtain flow is first shown in Fig. 2 in terms of volume fraction C (panels (a), (d), (g)), streamwise u (panels (b), (e), (h)) and spanwise w (panels (c), (f), (i)) liquid velocity components in xz plane. Note that the Weber number is equal to $We = 2.5$ for all the cases, while AR progressively reduces from the reference value $AR = 40$ discussed in previous Section 2.2 (first row of panels in Fig. 2), to $AR = 10$ (last row), with an intermediate value equal to $AR = 25$ (central row). The analysis of Fig. 2 clearly shows that, as AR decreases, the streamwise converging distance of the curtain rims also decreases, as an effect of the reduction in volumetric flow rate $Q^\star$. Moreover, a varicose mode progressively arises in xz plane, dramatically affecting the sheet configuration at $AR = 10$. This investigation reveals that, as a matter of fact, the curtain flow undergoes a transition from the typical triangular shape to a columnar jet regime as its aspect ratio decreases.

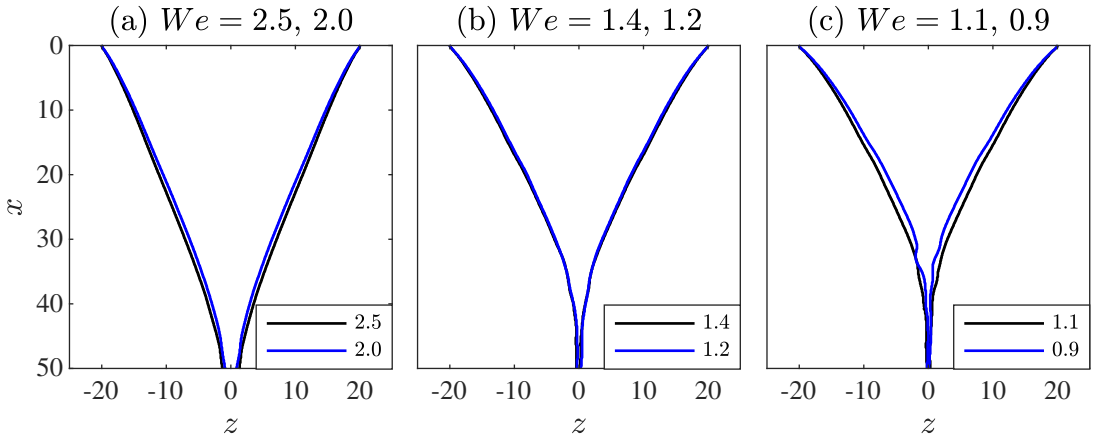

Figure 3: Slices of the liquid curtain interface in xz plane reducing the Weber number from supercritical ($We > 1$) to subcritical ($We < 1$) conditions. $AR = 40$.

3.2 Weber number effect

The Weber number variation in the analysis presented hereafter is achieved by reducing the inlet mean liquid velocity $U_i^\star$, i.e. by reducing the flowrate $Q^\star$ during the numerical simulation of the sheet flow. It is worth noting that this strategy, which is analogous to the standard experimental approach used to investigate the We effect on the curtain dynamics (among others, see de Luca [5], Finnicum *et al.* [6] and Le Grand-Piteira *et al.* [23]), implies the simultaneous variation of other two governing parameters, namely the Froude $Fr = U_i^{\star 2}/(gL^\star)$ and Reynolds $Re = \rho_l U_i^\star H_i^\star/(2\mu_l)$ numbers. Therefore, the physical mechanisms governing the supercritical ($We > 1$) to subcritical ($We < 1$) flow transition which will be here outlined strongly rely on the interplay among capillary, inertia, and viscous effects. In this respect, the present investigation differs from previous recent two-dimensional numerical simulations of the sheet flow, where the effect of one governing parameter at a time was analyzed (Della Pia *et al.* [19, 22] and Colanera *et al.* [20]).

Results of the investigation of the Weber number effect on the curtain dynamics are reported in Fig. 3, where frontal sections of the interface in xz plane are reported for different values of We ranging from supercritical ($We > 1$) to subcritical ($We < 1$) conditions. The competition between capillary retraction, determined by surface tension action on the edge rims, and flow inertia results in a reduction of the convergence length (i.e. the streamwise station where the sheet edges converge) and thinning of the curtain along the spanwise z direction as We decreases (Fig. 3(a)-(b)). Moreover, it is possible to appreciate that the curtain is able to maintain the classic triangular shape across the supercritical-to-subcritical transition, i.e. when the flow goes from $We = 1.1$ to $We = 0.9$, but in the latter case low amplitude sinuous spatial oscillations can be noted along the curtain tail (Fig. 3(c)). This abrupt modification of the sheet shape across the critical threshold ($We = 1$) is reminiscent of the so-called *frequency jump*, namely the discontinuous change in natural shape and oscillation frequency of a gravitational curtain in transcritical conditions, which has been found with a simplified linear low-dimensional analysis of liquid sheet sinuous modes (Della Pia *et al.* [21] and Girfoglio *et al.* [24]), and here outlined from 3D direct numerical simulation results. Further considerations regarding the frequency

jump of a three-dimensional curtain, and its relation with simplified low-dimensional model predictions, are provided in Appendix A. It is interesting to note that a behaviour analogous to the one depicted in Fig. 3(c) was identified in the experimental investigation by Le Grand-Piteira *et al.* [23], who studied spontaneous oscillations of two-dimensional liquid sheets falling from a horizontal wet tube and maintained between two vertical wires, finding that when We reduces below the unity a self-sustained chessboard pattern of sinuous waves abruptly arises on the sheet without disrupting it. From the latter point of view, the present analysis has revealed that a stable intact curtain can be maintained until $We = 0.8$, below which the formation of holes and their expansion start to arise, leading to the sheet rupture.

4 CONCLUSIONS

Three-dimensional two-phase direct numerical simulations have been carried out through the volume-of-fluid method to shed light on the flow of gravitational liquid curtains (sheets) issuing into an initially quiescent gaseous environment. In particular, the effect of the curtain aspect ratio AR and Weber number We on the sheet shape and dynamics have been characterized through a parametric investigation, providing comparisons with linear stability analysis predictions based on a simplified low-dimensional model of the flow.

The investigation has revealed a typical triangular regime of the curtain in supercritical conditions ($We > 1$) for $AR = 40$, and a transition from the triangular shape to a columnar regime when AR decreases, governed by the progressive excitation of a varicose mode. The analysis of We effect has outlined that the curtain is able to sustain the supercritical-to-subcritical flow transition without experiencing rupture, but undergoing a variation of shape and frequency when We crosses the critical threshold $We = 1$. The theoretical predictions of the sheet oscillations frequency as obtained from the simplified linear low-dimensional model (see Appendix A) are found to be valuable in comparison with the three-dimensional nonlinear simulations, both in supercritical ($We > 1$) and subcritical ($We < 1$) conditions.

A LINEAR STABILITY ANALYSIS OF THE CURTAIN FLOW

The flow transition from supercritical ($We > 1$) to subcritical ($We < 1$) conditions discussed in Section 3.2 is here further elucidated by showing the occurrence of a variation of the dominant curtain natural oscillation frequency when the Weber number reduces below the critical threshold $We = 1$, in the three-dimensional simulations, compared with its prediction made with a simplified low-dimensional model of the liquid sheet in xy plane. To realize this comparison, the VOF simulated meanline curtain within the xy plane is first defined as (see also Della Pia *et al.* [18])

$$\ell(x,t) = \frac{1}{\int_{-L/2}^{L/2} C(x,y,t)dy} \cdot \int_{-L/2}^{L/2} C(x,y,t)y\,dy. \tag{11}$$

Therefore, the natural oscillatory dynamics of the sheet flow in transcritical conditions is investigated by performing two direct numerical simulations, respectively for $We = 1.2$ and $We = 0.8$, and monitoring the temporal signal $\ell(x,t)$ at the station $x = 10$, namely at a streamwise location sufficiently far from the curtain rims convergence point. The normalized Fast Fourier Transform (FFT) of the sheet meanline temporal signal is shown in Fig. 4 for

supercritical (black dashed curve) and subcritical (blue dashed curve) conditions; it reveals a change of the dominant frequency (peak abscissa of the FFT) from $f^\star = 1.82$ Hz ($We = 1.2$) to $f^\star = 19.33$ Hz ($We = 0.8$), i.e. a relative percentage increase of the natural frequency equal to $\epsilon = 90.58\%$. This result agrees with predictions by linear stability analysis of the two-dimensional curtain natural frequency behaviour in transcritical conditions, which are also shown in Fig. 4 as vertical continuous lines ($f^\star_{LSA}$, relative percentage increase ϵ equal to 83.39%).

The values $f^\star_{LSA}$ of the sheet global oscillation frequency reported in Fig. 4 are the solutions of a boundary value eigenvalues problem, which is formulated enforcing the temporal global modes position in the following simplified set of linear equations modelling the curtain dynamics (Weinstein *et al.* [25], Della Pia *et al.* [21]):

$$v_m = \frac{\partial \ell_m}{\partial t} + u_{torr}\frac{\partial \ell_m}{\partial x_m}, \tag{12}$$

$$\frac{\partial v_m}{\partial t} + u_{torr}\frac{\partial v_m}{\partial x_m} = \frac{1}{WeH}\frac{\partial^2 \ell_m}{\partial x_m^2} + \frac{2\rho_a}{\pi\varepsilon\rho_l}\int_0^1 \frac{\partial^2 \ell_m}{\partial t^2}\ln|x_m - \xi|\, d\xi + \frac{\varepsilon}{2Re}\frac{\partial^2 v_m}{\partial x_m^2}, \tag{13}$$

where $\varepsilon = H_i^\star/L^\star$, $H = H^\star/H_i^\star$ is the dimensionless curtain local thickness, $t = t^\star U_i^\star/L^\star$ the dimensionless time, v_m is defined as $v_m = v^\star/(\varepsilon U_i^\star)$, $x_m = x^\star/L^\star$, ℓ_m is equal to $\ell_m = (y_m^+ + y_m^-)/2$ ($y_m^\pm$ being the two interface locations at a certain station x_m), $u_{torr} = \sqrt{1 + 2x/Fr}$ is the free-fall Torricelli base flow solution, and all other symbols have been already introduced within the text. This simplified model of the curtain flow is formulated under the assumptions of a nominally two-dimensional thin liquid sheet falling in still gaseous ambient under the action of gravity and subjected to such small perturbations to only excite the sinuous response of the flow, which turns out to be characterized by the meanline $\ell_m(x,t)$ and transverse velocity $v_m(x,t)$ dynamics only. Within these simplifications, Eqs. (12)-(13) represent the (dimensionless) linearized kinematic boundary condition and transverse momentum balance equation, respectively, accounting for viscous effects in the liquid phase ($\propto \partial^2 v_m/\partial x_m^2$) and for the curtain-ambient interaction ($\propto \int_0^1 \partial^2 \ell_m/\partial t^2 \ln|x_m - \xi|\, d\xi$).

Enforcing the temporal normal mode position in Eqs. (12)-(13), $\ell_m(x,t) = \hat{\ell}(x)\cdot e^{\lambda t}$ and $v_m(x,t) = \hat{v}(x)\cdot e^{\lambda t}$, the following eigenvalue problem is obtained

$$\lambda \begin{bmatrix} \mathrm{I} - RU\cdot\mathcal{I} & RU\cdot\mathcal{I}\cdot U\cdot\mathcal{D} \\ \mathcal{O} & \mathrm{I} \end{bmatrix} \begin{Bmatrix} \hat{v} \\ \hat{\ell} \end{Bmatrix} = \begin{bmatrix} -U\cdot\mathcal{D} + \dfrac{\varepsilon}{2Re}\mathcal{D}^2 & \dfrac{U}{We}\mathcal{D}^2 \\ \mathrm{I} & -U\cdot\mathcal{D} \end{bmatrix} \begin{Bmatrix} \hat{v} \\ \hat{\ell} \end{Bmatrix}, \tag{14}$$

which allows one to compute complex eigenvalues (λ) and eigenfunctions ($\hat{\ell}$, $\hat{v}$) with spectral accuracy by means of a Chebyshev collocation method in MATLAB. In Eq. (14), I denotes the identity operator, $\mathcal{D}$ and $\mathcal{D}^2$ represent first and second order spatial derivatives, respectively, U is a diagonal matrix containing u_{torr} values, the coefficient R is equal to $R = 2\rho_a/(\pi\varepsilon\rho_l)$, and $\mathcal{I}$ is the integral operator $\mathcal{I} = \int_0^1(\cdot)\ln|x-\xi|\, d\xi$. The imaginary part of the eigenvalue $\lambda = \lambda_r + i\lambda_i$ characterized by the maximum growth rate λ_r represents the global (dimensionless) oscillation frequency, and it is related to $f^\star_{LSA}$ by the relation $\lambda_i = 2\pi f^\star_{LSA} L^\star/U_i^\star$. The enforcing of boundary conditions for the system (12)-(13), together with the physical interpretation of the

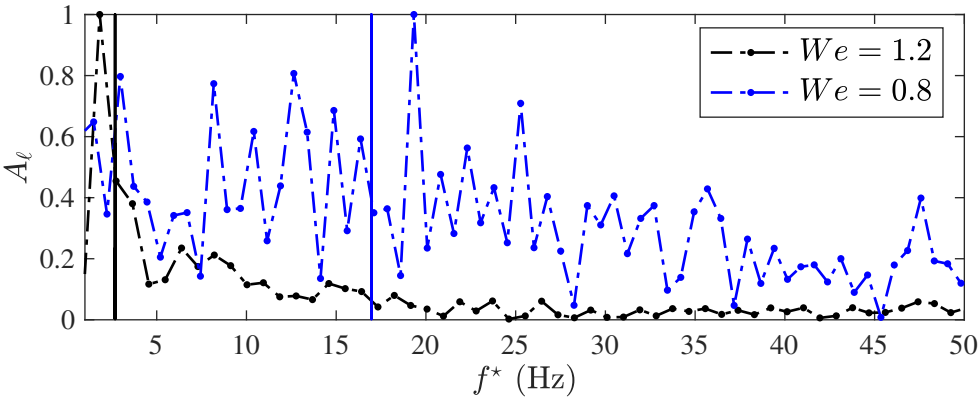

Figure 4: Normalized FFT of the sheet meanline temporal signal $\ell(x,t)$ in xy plane in supercritical (black dashed curve) and subcritical (blue dashed curve) conditions at $x = 10$ ($AR = 40$). The global oscillation frequencies predicted by linear stability analysis for $We = 1.2$ ($f^\star_{LSA} = 2.68$ Hz, black vertical line) and $We = 0.8$ ($f^\star_{LSA} = 16.96$ Hz, blue vertical line) are also reported.

eigenvalues spectrum, are extensively discussed in Della Pia *et al.* [21], and therefore not repeated herein.

REFERENCES

[1] Soderberg, L. D. and Alfredsson, P. H. Experimental and theoretical stability investigations of plane liquid jets. *European Journal of Mechanics - B/Fluids* (1998) **17**:689–737.

[2] Weinstein, S. J. and Ruschak, K. J. Coating flows. *Annual Review of Fluid Mechanics* (2004) **36**:29–53.

[3] Chubb, D. L., Calfo, F. D., McConley, M. W., McMaster, M. S. and Afjeh, A. A. Geometry of thin liquid sheet flows. *AIAA Journal* (1994) **32**:1325–1328.

[4] Lodomez, M., Crookston, B. M., Tullis, B. P. and Erpicum, S. Mitigation Techniques for Nappe Oscillations on Free-Overfall Structures. *Journal of Hydraulic Engineering* (2019) **145**(2):04018086.

[5] de Luca, L. Experimental investigation of the global instability of plane sheet flows. *Journal of Fluid Mechanics* (1999) **399**:355–376.

[6] Finnicum, D. S., Weinstein, S. J. and Rushak, K. J. The effect of applied pressure on the shape of a two-dimensional liquid curtain falling under the influence of gravity. *Journal of Fluid Mechanics* (1993) **255**:647–665.

[7] Torsey, B., Weinstein, S. J., Ross, D. and Barlow, N. The effect of pressure fluctuations on the shapes of thinning liquid curtains. *Journal of Fluid Mechanics* (2021) **910**:A38-1–A38-14.

[8] Brown, D. R. A study of the behaviour of a thin sheet of moving liquid. *Journal of Fluid Mechanics* (1961) **10**:297–305.

[9] Scardovelli, R. and Zaleski, S. Direct numerical simulation of free-surface and interfacial flow. *Annual Review of Fluid Mechanics* (1999) **31**(1):567–603.

[10] Hirt, C. W. and Nichols, B. D. Volume of fluid (VOF) method for the dynamics of free boundaries. *Journal of Computational Physics* (1981) **39**(1):201–225.

[11] Francois, M. M., Cummins, S. J., Dendy, E. D., Kothe, D. B., Sicilian, J. M. and Williams, M. W. A balanced-force algorithm for continuous and sharpe interfacial surface tension models within a volume tracking framework. *Journal of Computational Physics* (2006) **213**(1):141–173.

[12] van Hooft, J. A., Popinet, S., van Heerwaarden, C. C., van der Linden, S. J. A., de Roode, S. R. and van de Wiel, B. J. H. Towards adaptive grids for atmospheric boundary-layer simulations. *Boundary-Layer Meteorology* (2018) **167**(3):421–443.

[13] Popinet, S. Gerris: a tree-based adaptive solver for the incompressible Euler equations in complex geometries. *Journal of Computational Physics* (2003) **190**(2):572–600.

[14] Popinet, S. An accurate adaptive solver for surface-tension-driven interfacial flows. *Journal of Computational Physics* (2009) **228**(16):5838–5866.

[15] Kacem, A. Étude expérimentale et numérique d'une nappe liquide en écoulement gravitaire. *Thèse de doctorat en Mécanique des fluides, Université de Pau et des Pays de l'Adour, http://www.theses.fr/2017PAUU3052* (2017).

[16] Kacem, A., Le Guer, Y., El Omari, K., Bruel, P. Experimental investigations of planar water sheets flowing under gravity. *WIT Transactions on Engineering Sciences* (2017) **115**:97–107.

[17] Agbaglah, G. G. Breakup of thin liquid sheets through hole-hole and hole-rim merging. *Journal of Fluid Mechanics* (2021) **911**(A23).

[18] Della Pia, A., Chiatto, M. and de Luca, L. Global eigenmodes of thin liquid sheets by means of Volume-of-Fluid simulations. *Physics of Fluids* (2020) **32**(082112).

[19] Della Pia, A., Chiatto, M. and de Luca, L. Receptivity to forcing disturbances in subcritical liquid sheet flows. *Physics of Fluids* (2021) **33**(032113).

[20] Colanera, A., Della Pia, A., Chiatto, M., de Luca, L. and Grasso, F. Modal decomposition analysis of unsteady viscous liquid sheet flows. *Physics of Fluids* (2021) **33**(092117).

[21] Della Pia, A., Colanera, A., Chiatto, M. and de Luca, L. Energy insights into the unsteady dynamics of a viscous gravitational liquid sheet. *Physics of Fluids* (2021) **33**(092118).

[22] Della Pia, A., Colanera, A. and Chiatto, M. Surface tension-induced instability in spatially developing subcritical liquid curtains. *Physics of Fluids* (2022) **34**(042122).

[23] Le Grand-Piteira, N., Brunet, P., Lebon, L. and Limat, L. Propagating wave pattern on a falling liquid curtain. *Physical Review E* (2006) **74**(026305).

[24] Girfoglio, M., De Rosa, F., Coppola, G. and de Luca, L. Unsteady critical liquid sheet flows. *Journal of Fluid Mechanics* (2017) **821**:219–247.

[25] Weinstein, S. J., Clarke, A., Moon, A. G. and Simister, E. A. Time-dependent equations governing the shape of a two-dimensional liquid curtain, Part 1: Theory. *Physics of Fluids* (1997) **9**(12):3625–3636.